Incidence Angle and Diffuse Radiation Adaptation of Soiling Measurements

F. Wolfertstetter,[1, a)] A. Esquelli,[2] S. Wilbert,[1] N. Hanrieder,[1] M. Korevaar,[3] T.Bergmans,[3] and A. Ghennioui[4]
[1)] *DLR, Institute of Solar Research, Paseo de Almeria 73, 04001 Almeria, Spain*
[2)] *Berlin University of Technology, Renewable Energy Systems, Straße des 17. Juni 135, 10623 Berlin, Germany*
[3)] *Kipp & Zonen, Meteorology Division of OTT HydroMet, Delftechpark 36, 2628 XH Delft, Netherlands*
[4)] *IRESEN, Green Energy Park, Route Régionale Kelaa Km 3 R206, Ben Guerir, Morocco*

(Dated: 16 November 2020)

Soiling is responsible for a loss of 3-4% of the potential global solar power production that is estimated to rise because of increased deployment in dusty environments.[1] For effective mitigation strategies and site selection soiling ratio data is crucial. In recent years, a number of automatic sensors such as Kipp and Zonen's DustIQ that we employ in this study, have been introduced to the market that do not use PV cells to determine the soiling ratio. As the DustIQ detects a scattering signal from a proprietary light source its signal does not depend on the solar position. The soiling-induced output power loss of PV reference cells show an incidence-angle dependent pattern. In diffuse lighting conditions as caused by clouds or haze, the response of the soiled modules depends less on the sun angle.

We present an analysis of the AOI-dependency of the reference cell soiling ratio taking into account the irradiance conditions during measurement. Based on the analysis of AOI dependence we propose a method to correct the soiling measurement signal of automatic, incidence-angle independent soiling sensors using the angle of incidence and the Linke Turbidity, derived from GHI and DNI measurements, as inputs to the adaptation function. The method can improve performance analysis that considers soiling measurement data as an input. If the AOI-dependency is not taken into account, the daily power production of a solar panel or farm can be overestimated significantly, especially for plants with oversized PV arrays.

I. INTRODUCTION

The transmission of incident light on fixed tilted PV systems depends on the angle of incidence (AOI or θ)[2–6]. This effect, often referred to as 'cosine effect' depends on the sun's position in the sky and atmospheric conditions. Before reaching the semi-conductor, the incident sunlight has to pass an air/glass and glass/encapsulant interface, causing parts of the incident light to be reflected, absorbed or transmitted. Reflection between the layer's boundaries increase with increasing angle of incidence[7]. The transmittance of the PV cover depends on the angle-dependent refraction that takes place at these interfaces. The AOI-dependency is additionally influenced by the angle dependent absorption coefficient of the solar cell material.

When dust accumulates on the PV surface, it changes the optical behaviour of the air/glass interface. The impact of the angle of incidence grows with increasing particle density as larger portions of direct incident light are being absorbed or scattered by the dust particles.

The issue of PV soiling losses linked to the AOI effect has been object of several studies. Efforts were mainly made to derive empirical models with which it is possible to quantify the daily variable losses.

Zorilla-Casanova et al.[4] studied the energy losses due to accumulated dust on PV surfaces, determining soiling losses with two reference devices. They concluded that summing up daily losses over a whole year can lead to a decrease of the total energy production of about 4.4 %. They also examined the peculiar shape of the curve of the dust-caused irradiance losses in dependence of the angle of incidence. At noon minimal soiling losses for the day were observed with an increase up to a maximum value found at 75° incidence and a decrease of losses for larger incidence angles, which they explained by the influence of the higher diffuse fraction of the irradiance at these large angles.

Martin and Ruiz[2] introduced a functional relationship between the angular losses (AL) of PV modules and the angle of incidence and tested the model on different module types. The model equation includes an AOI dependent spectrally weighted transmittance term, which describes the integrated angular behaviour of distinctively coated PV cells. In order to derive a change in AOI dependent optical behaviour, an angular factor can be calculated, building the ratio between weighted transmittance at a specific AOI and at normal incidence, the latter giving the maximum transmittance and is commonly specified by the manufacturer. The angular factor can also be calculated experimentally through the ratio of the measured short-circuit current at a specific AOI to the short-circuit current at normal incidence times the cosine of the angle. A dimensionless angular loss coefficient a_r has to be determined experimentally for each technology. In order to determine the AOI effect of soiled devices, a_r can be fitted for different soiling densities[8]. The incidence angle modifier $1 - AL$ gives the attenuation of the response with increasing angle of incidence. The attenuation of the response increases with increasing a_r. Even though this model does provide information on the angular losses expressed through the influence of the AOI in attenuating a module's short-circuit-current, it does not quantify the losses caused exclusively by soiling.

Soiling measurements are often performed using two iden-

[a)] corresponding author; fabian.wolfertstetter@dlr.de; www.dlr.de/sf

tical PV reference cells (PVRC) which are installed side by side, being representative for a PV installation in terms of mounting and material properties. One is left to long term soiling exposure and one is cleaned every day. The ratio of the power outputs of both devices successively decreases with the soiling level of the surfaces. This ratio is called soiling ratio or cleanliness, denoted ξ. It is dependent on angular losses caused by the cosine effect and the diffuse contribution for flat AOI, which in turn depend on the soiling density deposited on the sample surfaces.

Nepal et al.[9] made use of the model developed by *Martin and Ruiz*[2,8] by parametrizing the angular loss coefficient a_r in dependence of the soiling ratio and calculating the incidence angle modifier of the soiled sample with the corresponding a_r. The derived empirical model based on the incidence angle modifier and a single soiling ratio measurement value at solar noon led to an accurate prediction of $\pm$ 0.21 % for a sunny day, whereas in shady conditions the deviation was higher.

Relative measurements with two PV reference devices have proven to be efficient to quantify soiling losses. *Dunn et al.*[10] could show in their comparison analysis of pyranometers and PVRCs, that the latter provide superior irradiance measurements for PV power plant monitoring applications with uncertainties on the order of +/- 2.4% compared to +/- 5% when using thermopile pyranometer measured irradiance. In a later study, they approximated the absolute uncertainty of soiling ratio measurements with PVRCs to about $\sim$ +/-1% around solar noon, which is acceptable for qualitative as well as quantitative soiling loss determination[11]. It also was suggested to minimize the biases through filtering data to include only measured irradiance values occurring within a few hours of solar noon, when the AOI is at its lowest and averaging equal portions of data before and after solar noon of each day. However, this would leave irradiance values in the range of high AOI uncorrected if a constant influence of the soiling layer is assumed.

Performing soiling measurements with PVRCs at utility-scale is nowadays the most precise method to quantify soiling losses under operating conditions. However, since daily or weekly cleaning of one of the devices is mandatory, eliminating this requirement in order to measure soiling would enhance maintenance in terms of cost effectiveness and water savings. On the other hand, already commercialized maintenance-free soiling measurement solutions such as the DustIQ, an optical soiling measurement device manufactured by *Kipp & Zonen*[12], or Atonometrics' MARS sensor, neglect physical phenomena such as angular effects and the influence of the diffuse irradiance on the soiling ratio. An AOI-adaptation of these devices for a specific PV system enables operators to determine soiling losses at a specific time of the day, and derive a more accurate daily average value as suggested by the International Electrotechnical Commission (IEC) norm 61724-1:2017[13]. In the present work an adaptation method that takes the AOI effect and the diffuse contribution into consideration will be developed. For this purpose, the optical response of a fix tilted PVRC soiling measurement setup will be evaluated and compared to the adjacently installed DustIQ. The method will be applied and validated for measurement data from two solar research facilities: CIEMAT's Plataforma Solar de Almería (PSA) in Spain and IRESEN's Green Energy Park (GEP) in Ben Guerir/Morocco.

II. MATERIALS AND METHODS

In the following we describe the soiling measurement devices and data processing applied in this study. To determine the soiling-related transmission losses of a PV cell, measurements with tilted PVRCs at the PSA's KONTAS meteo station have been evaluated. The set-up consist of two pairs of 50 x 50 mm^2 monocrystalline silicon, one pair covered with smooth and the other with standard textured PV solar glass[14]. The cells can be seen in the left picture of Figure 1 at the upper right corner of the PV panels that are not analyzed for this study. Soiling ratio measurements with the DustIQ installed on the top left corner of the solar panels will be compared to the PVRCs, as it is mounted on the same height and thus should be subject to similar dust deposition. All PV measurement devices are inclined approximately 45° and are oriented in South direction.

The soiling measurement at GEP in Ben Guerir is shown in the right picture in Figure 1. It is composed of two monocrystalline PV modules and a co-planar DustIQ with an inclination angle of 30° and south orientation.

FIG. 1. Measurement setup. Left picture (at CIEMAT's PSA) - Fixed PVRC and DustIQ's installed with a tilt of 45° facing south. Right picture (at IRESEN's GEP) - Two solar modules and DustIQ mounted with a tilt of 30° facing south.

A. PV reference cell soiling setup

PV reference cells (PVRCs) are used to determine the irradiance in the plane of array (POA) through the measurement of the short-circuit current. The short-circuit-current is converted to a voltage signal through a 0.1 Ohm shunt resistor. This signal shows a linear correlation to the POA irradiance in the range of 50 to 1500 W/m² with a corresponding signal voltage of 95 mV (+/- 8 %) at 1000 W/m², as specified on the manufacturers data sheet[14]. The measurement set-ups at the PSA and the GEP correspond to measurement method two specified in the IEC 61724-1 named *short-circuit current reduction due to soiling*[13]. An overview of the measurement setup is given in Figure 2. The short-circuit-current of single cells is proportional to the generated power output. The IEC on soiling measurements defines the PV cell's soiling ratio as

the ratio of the actual power output P of a soiled to an identical but clean PV sample[13]. Because the power output of a PV cell is proportional to the irradiance G it detects, the soiling ratio can be measured with the described setup according to definition:

$$\xi = \frac{P_s}{P_c} = \frac{i_{sc,s}}{i_{sc,c}}, \tag{1}$$

where indices s and c indicate soiled and clean reference cells. The soiling ratio is measured in 1-minute resolution. A calibration to convert the signal of the cells to POA irradiance $G_{\beta,\gamma}$ has been performed by the manufacturer by comparison to an identical reference cell at 800 $W/m^2 < G_{\beta,\gamma} <$ 1000 W/m^2. The calibration was performed around solar noon under clear sky conditions.

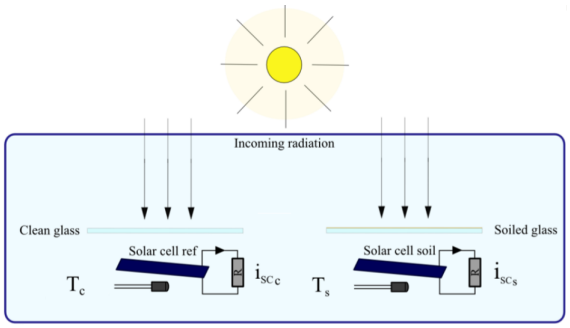

FIG. 2. PV soiling measurement principle using two PVRC's at the KONTAS meteo station within CIEMAT's PSA.

An integrated PT100 temperature sensor records the devices temperature for temperature correction of the irradiance signal according to:

$$G_{\beta,\gamma} = i_{sc}(1 - \alpha_T(T - T_{ref})) \cdot \frac{G_{\beta,\gamma,ref}}{i_{sc,ref}}, \tag{2}$$

where α_T is the cell's temperature coefficient provided by the manufacturer and $i_{sc_{cal}}$ is the short-circuit current measured during the calibration at a reference irradiance value G_{ref} of 1000 W/m^2 and a reference temperature T_{ref} of 25 °C (STC), as specified by the manufacturer[15].

At the GEP, PV modules are used as reference devices. The soiling ratio has been calculated using the short-circuit-currents measured in 1-minute resolution of both modules according to equation 1. For both setups a temperature correction has been applied to the current measurements analogous to equation 2:

$$i_{sc} = i_{sc,raw}(1 - \alpha_T(T - T_{ref})) \tag{3}$$

where $i_{sc,raw}$ is the raw measurement signal and i_{sc} is used to determine the soiling ratio above.

At CIEMAT's PSA, data was collected from the 14.06.2018 until the 14.06.2019. The two upper cells were cleaned every day between 8:30 and 9:30 a.m., the two lower cells were cleaned after several months of soiling exposure. At GEP, data was collected from the 01.03.2018 until the 31.12.2018.

Figure 3 shows PV soiling ratio measurements under sunny and shady conditions. For sunny conditions, there is a clear dependency of the soiling ratio on the time of the day and the angle of incidence. For shady instants (cloudy or turbid atmosphere) the influence of AOI on the soiling ratio is significantly reduced, due to the fact that the diffuse contribution has negligible angular dependence. The measured soiling ratio is noisier but stays on a constant level, as shown in the right plot. Sudden leaps of the soiling ratio, as they occur on the right plot in figure 3 around 9:30, can be caused by rapidly changing irradiance conditions as can be caused by passing clouds.

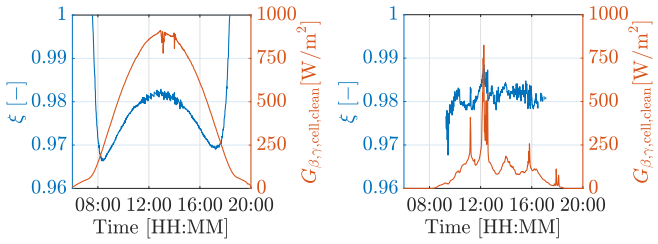

FIG. 3. Soiling Ratio ξ in blue and corresponding $G_{\beta,\gamma}$ of the clean cell at the PSA for the textured PV cell pair for a sunny (left) and cloudy day (right).

Other sources of uncertainty for soiling ratio measurements with PVRCs can be linked to remaining non-linearity of irradiance measurements, misalignment errors and moving clouds.

The effect of discrepancies in the angular alignment of the clean and soiled tilted modules result in a bias in soiling ratio measurement. Differences between the PVRC azimuth angles result in a drift of the measured soiling ratio during the day, as one sample faces more towards the morning or evening sun than the other. In the frame of this study an angular misalignment correction method was carried out, using a site dependent transposition model for the exact south as reference to correct the output signals of the clean and soiled PVRC samples.

B. DustIQ sensor

The DustIQ is a novel optical soiling monitoring device that has been introduced to the market by *Kipp & Zonen* in 2018. Through its compact design the device can be easily mounted in the plane of an operating PV field such that it is subject to similar soiling conditions and same cleaning actions as the solar panels. The installation of multiple DustIQ's can give an overview on soiling occurring in different parts of the PV plant, thus complying with IEC requirements[13]. It derives the soiling ratio based on the detection of the scattered portion of a pulsed infrared light source as depicted in figure 4.

The raw photodiode measurement is converted to the soiling ratio using a calibration constant. The latter is dependent on the optical properties of the dust in question: different size distributions and scattering coefficients will have higher scattering to absorption coefficients. Especially the dust color has

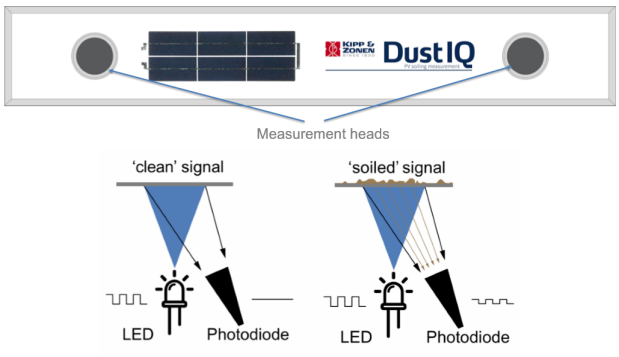

FIG. 4. Soiling measuring principle with the DustIQ[16]

a major impact on the amount of scattered light and depends on local dust properties[17]. Therefore, a dust slope calibration using the internal PV cells of the device is recommended that adapts the factory calibration to the local dust properties. The local DustIQ calibration requires a previous exposure to local soiling conditions, resulting in an evenly distributed dust layer on the DustIQ surface corresponding to a soiling ratio of 90-95 %. The calibration has to be performed within two hours of local solar noon, having a clear view on the sun and the sky for at least 15 minutes with at least 800 W/m^2 solar irradiance[18]. It consists of step-wise cleaning of the on-board solar cells and the measurement surfaces. The difference in soiled and cleaned output signals from the photodiode is then correlated to the soiling ratio detected using the on-board PV cells at the moment of the calibration. The dust slope calibration of the DustIQ has been performed on June 14th of 2019 at a solar incidence angle of $AOI_{\text{ref,PSA}} = 34°$ at CIEMAT's PSA. At GEP, the factory calibration has been applied for dataprocessing in the DustIQ and no local dust calibration has been performed. The reference AOI has been chosen as $AOI_{\text{ref,GEP}} = 26°$. Technical specifications of the DustIQ can be found in the following table:

TABLE I. DustIQ specifications (source: *Kipp & Zonen*)

Soiling ratio uncertainty 100% - 90%	+/- 1 %
Soiling ratio uncertainty 90% - 80%	+/- 2 %
Soiling ratio uncertainty 80% - 50%	+/- 5 %
Ambient temperature range	-20 to +60 °C
Weight	5 kg
Instrument dimensions	990 x 160 x 40 mm

III. INCIDENCE ANGLE DEPENDENCY AND ADAPTATION METHOD

A. Data comparison

Assuming that the DustIQ and PVRCs have accumulated similar soiling layers and that the calibration works correctly, both soiling measurements should coincide at the reference AOI interval of the DustIQ calibration. Two measurement intervals with data for the soiling ratios of the PVRC pairs and the DustIQ signals as well as the AOI are shown in figure 5. The DustIQ soiling ratio from August 2018 shown on the left plot corresponds to the factory calibration, performed by the manufacturer before shipment. The right plot shows data processed with the local dust calibration. The latter was performed on the 14th of June 2019 and applied retrospectively to all DustIQ data from the 29th of January 2019 and onwards. The general trend of the soiling ratio shows a similar behaviour in both plots, the absolute values show a deviation of up to 0.02 for AOIs further off the reference AOI interval before the calibration and up to 0.01 for data processed with the local dust calibration. The curves of DustIQ and the PVRC pairs coincide at similar AOI, but the DustIQ does not reproduce the daily pattern of the PVRC pairs.

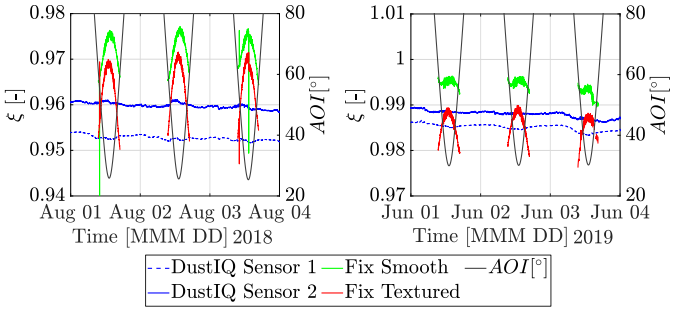

FIG. 5. DustIQ vs. fixed smooth and textured PVRC soiling ratio for $G_{\beta,\gamma}$ values greater 500 W/m^2 at CIEMAT's PSA. Left plot - Three exemplary days in August 2018, before the local dust slope calibration. Right plot - Three exemplary days in June 2019, after the local dust slope calibration.

At CIEMAT's PSA, the AOI effect for the textured tilted PVRC was found to reach up to 2 % in summer 2018 when considering incident global tilted irradiance greater than 500 W/m^2. For the smooth cells the daily variation reached about 1 %, as even small particles can be re-suspended more easily from its surface.

At IRESEN's GEP, the AOI effect reached almost 8 % in summer 2018 due to more pronounced dust accumulation on the module surface corresponding to a soiling ratio of roughly 80 %, see figure 6. This supports the argument, that the AOI effect increases with increased dust density deposited on the PV module surface. The morning peaks in the dustIQ signal are caused by dew droplets on the measurement surface that temporarily increase the scattering signal. DustIQ data affected by dew is excluded in the comparisons below.

The higher deviation between the soiling ratios of the module and the DustIQ around solar noon is represented in the specified uncertainties for the DustIQ for soiling ratios between 50 % and 80 % (see table I). Also, uncertainties in soiling ratio measurements with the PV modules have to be taken into consideration. Due to the PV module's larger area, soiling can be distributed heterogeneously to cause mismatch effects. Additionally, dust deposition and natural cleaning events might be biased for small and large surfaces.

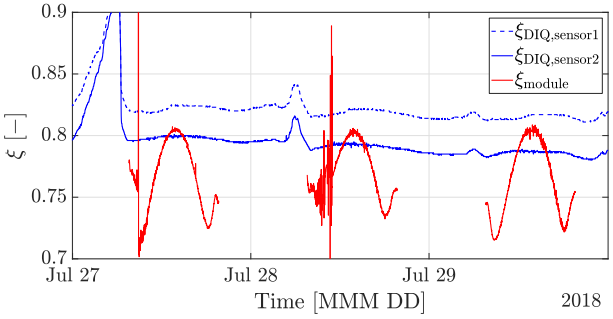

FIG. 6. DustIQ vs. PV module soiling ratio at GEP

B. Energy weighted analysis of AOI influence

In the next step we analyze the influence of changing beam and diffuse portions of incident light on the PVRC soiling ratio measurement as can be found during shady or hazy conditions. Furthermore we will analyze the effect of the AOI-dependent soiling-effect on power production.

The global solar irradiance received by a tilted solar cell depends on geophysical factors including changes in climate and the surfaces positioning, characterized by the local altitude, its inclination angle β and the solar-surface azimuth angle γ. The global tilted irradiance $G_{\beta,\gamma}$ is split into a beam $B_{\beta,\gamma}$, a diffuse $D_{\beta,\gamma}$ and a ground reflected $R_{\beta,\gamma}$ component, giving the following general transposition model equation[19]:

$$G_{\beta,\gamma} = \underbrace{\mathrm{DNI}\cdot\cos\theta}_{B_{\beta,\gamma}} + \underbrace{\mathrm{DHI}\cdot \mathrm{R_d}}_{D_{\beta,\gamma}} + \underbrace{\mathrm{GHI}\cdot R_\mathrm{r}\cdot\rho_g}_{R_{\beta,\gamma}}, \tag{4}$$

where $\mathrm{R_d}$ is the factor of diffuse reflectance calculated using the *Ma-Iqbal*[20] anisotropic model combining isotropic and circumsolar radiation. This model has been found to be the best performing at the PSA and several climatically comparable areas. The ground reflected contribution $R_{\beta,\gamma}$ is proportional to GHI. While R_r is exclusively calculated through the surface inclination, the definition of the ground albedo requires additional input. Actually, the ground reflectance is dependent on the locations climatic conditions, humidity and daytime being the most influential factors. In this study the definition of a constant value for the ground albedo is sufficient considering the low contribution of the ground reflectance to the global tilted irradiance at 45° and 30°. A value of 0.32 for the PSA and the GEP, given by the mean of the albedo values of a desert scape (0.4) and grassland (0.25), are assumed in this study[21].

The average yearly contribution of the beam portion $B_{\beta,\gamma}$ to the total irradiance on the POA is calculated dividing the integral of the irradiance component over time intervals in AOI bis (AOI_i) by the integral over $G_{\beta,\gamma}$:

$$w_{\mathrm{Beam},AOI_i} = \frac{\int_{t|AOI_i(t)} B_{\beta,\gamma}(t)\,\mathrm{d}t}{\int_{t|AOI_i(t)} G_{\beta,\gamma,\mathrm{tot}}(t)\,\mathrm{d}t} \tag{5}$$

The AOI bin specific energy weights for the total diffuse portion $w_{\mathrm{Diffuse,tot}}$ are calculated analogously:

$$w_{\mathrm{Diffuse,tot},AOI_i} = \frac{\int_{t|AOI_i(t)} D_{\beta,\gamma}(t) + R_{\beta,\gamma}(t)\,\mathrm{d}t}{\int_{t|AOI_i(t)} G_{\beta,\gamma,\mathrm{tot}}(t)\,\mathrm{d}t}, \tag{6}$$

The energy weights of the shady diffuse portion $w_{\mathrm{Diffuse,shady}}$ has been calculated through eq. (6) filtering out all sunny events. Details of the employed cloud checker are given in the next section. The energy weights of the sunny diffuse contribution can finally be calculated as:

$$w_{\mathrm{Diffuse,sunny},AOI_i} = w_{\mathrm{Diffuse,tot},AOI_i} - w_{\mathrm{Diffuse,shady},AOI_i} \tag{7}$$

The energy weights and their cumulative sums for each irradiance component as well as for $G_{\beta,\gamma}$ at the PSA are represented in ascending 5° AOI_i-bins in figure 7 and for GEP see figure 8.

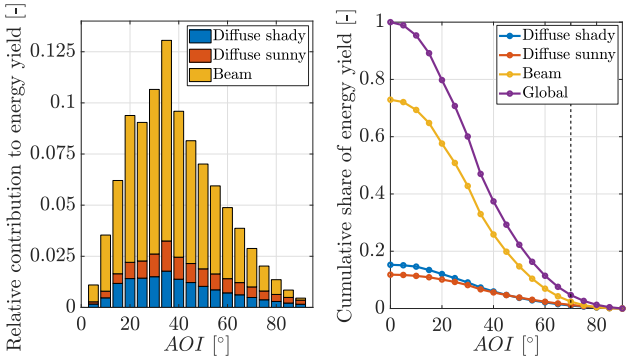

FIG. 7. Energy weighted AOI distribution for the PV cells oriented 45°, South at CIEMAT's PSA - relative contributions (left, stacked) and cumulative share (right)

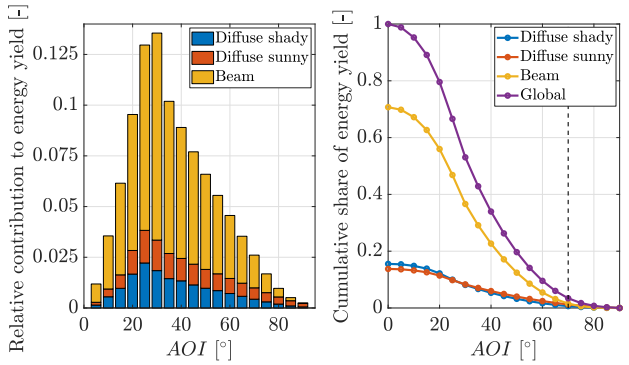

FIG. 8. Energy weighted AOI distribution for the PV cells oriented 30°, South at IRESEN's GEP - relative contributions (left, stacked) and cumulative share (right)

Considerable shares of energy production are generated at large AOI. At the 45°-South configuration at CIEMAT's PSA, approximately 57 percent of the global tilted irradiance are received at AOI's between 30° and 75°. The beam portion contributes the largest share in the yearly produced energy.An AOI adapation of active soiling sensors is therefore more important at sites with high direct irradiance shares.

C. Cloudy instants identification with the Linke turbidity

As we have to separate sunny from shady instances due to the resulting discrepancy in soiling loss behaviour, an adequate parameter has to be used in order to identify cloudy or highly turbid instants. Several indicators have been derived to approximate atmospheric absorption and scattering of the solar radiation under clear skies through measurements of the diffuse or direct solar contribution[22–24]. The Linke turbidity coefficient T_L is a measure of the atmosphere's optical thickness characterized by the amount of absorbed and scattered sunlight relative to the amount of sunlight that would reach the ground if the direct beam would pass through a clean and dry atmosphere. It can be calculated as follows[22]:

$$T_{\mathrm{L}} = \frac{1}{-\delta_{\mathrm{cda}} \cdot AM} \cdot \ln\left(\frac{DNI}{I_{\mathrm{E}}}\right) \tag{8}$$

where the optical thickness of a clean and dry atmosphere δ_{cda} is defined as follows:

$$\delta_{\mathrm{cda}} = (9.4 + 0.9 \cdot AM)^{-1} \tag{9}$$

where the Air Mass (AM) is the direct optical path length through the Earth's atmosphere relative to the vertical path, it has been described, e.g. by *Kasten and Young*[25].

An algorithm that detects cloudy and highly turbid instants has been presented in[26,27], using T_L and DNI measurements as input. Figure 9 shows an example of measured DNI, derived T_L and the according cloud filtered DNI data points in 1 minute resolution:

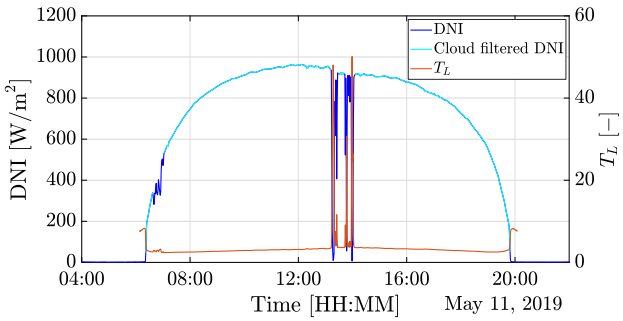

FIG. 9. Cloud and turbid atmosphere filtered DNI with cloud-checker algorithm, recorded at the PSA, method by[26,27]

The respective boundaries used in this algorithm as input parameters have been set to detect instants when a cloud shades the sun at the PSA. The filter is applied for solar elevation angles greater than 3°. A cloud is detected when one of the two following criteria is fulfilled:

- The Linke turbidity is greater than 13 for solar elevations greater than 5° and greater than 10 for solar elevations lower than 5°.
- The temporal variability ΔT_L is greater than 0.06 per minute.

The threshold of the variability is a rather conservative value, which leads to a small fraction of highly turbid sunny data points being filtered out.

D. Beam exposed cell incidence angle dependency

In order to represent AOI dependent optical losses caused by soiling, the daily soiling ratio trends recorded over the entire observed time frame have to be normalized around a selected site specific AOI reference interval. We determine the ratio of the soiling ratio ξ_{cell} for a given AOI and the average soiling ratio $\bar{\xi}_{\mathrm{cell},AOI\mathrm{ref}}$ measured on the same day for a given AOI interval:

$$\xi_{\mathrm{cell,norm}} = \frac{\xi_{\mathrm{cell}}}{\bar{\xi}_{\mathrm{cell},AOI\mathrm{ref}}} \tag{10}$$

The AOI reference bin, which is used to normalize the daily curves of the recorded soiling ratio values, generally has the highest energetic weighting, since it occurs over the entire year. At PSA, for a maximum solar elevation angle of approximately 76° and a surface with a tilt angle of 45° facing south, the minimum AOI (solar noon) is about 31° which results in a finally selected AOI reference bin including soiling ratio values measured at AOI between 32° - 36° with a reference AOI of 34 ° corresponding to the time the local dust calibration of the DustIQ has been performed. At the GEP, we select an AOI reference interval of 24° - 28° with an AOI_{ref} of 26°.

In figure 10 the normalized soiling ratio is represented over the AOI for the fixed cells with textured cover glass for cases in which the sun was not masked by a cloud. Shady instants are filtered out with the cloud-checker algorithm. The colorbar shows daily average soiling ratios $\bar{\xi}_{\mathrm{cell},AOI\mathrm{ref}}$. Days with high variance of soiling rate within AOI_{ref} are filtered out since $\bar{\xi}_{\mathrm{AOIref}}$ might not be representative for the respective day and would lead to inaccurate fitting results.

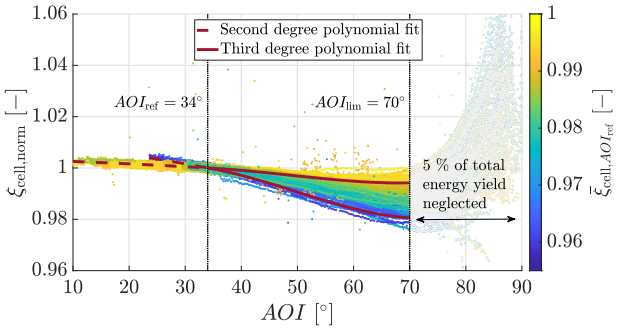

FIG. 10. Normalized T_L-cloudfiltered soiling ratio vs. AOI with color coded $\bar{\xi}_{\mathrm{cell},AOI\mathrm{ref}}$ and exemplary fits through selected $\bar{\xi}_{\mathrm{cell},AOI\mathrm{ref}}$ for the fixed cells with textured glass cover under sunny conditions at the PSA

In order to determine a functional relationship between the optical influences caused by soiling and the AOI, we fit polynomials f of order 2 for AOI smaller AOI_{ref} and of order 3 for AOI greater AOI_{ref} as a function of the AOI for given 0.005 wide $\bar{\xi}_{\mathrm{cell},AOI\mathrm{ref}}$ bins. The fits are forced to 1 at 34°. The narrower the soiling ratio bins the higher the accuracy of the fit for the respective soiling level. In figure 10 two exemplary fits for two different $\bar{\xi}_{\mathrm{cell},AOI\mathrm{ref}}$ bins are shown. Given the high measurement uncertainty around sunrise and sunset, the data

with AOI greater than 70° corresponding to ∼ 5% of the total yearly energy yield (see figure 7) are not included in order to keep fit quality high.

At GEP, higher soiling levels are measured. We apply the fits and filters described above. In figure 11 the normalized soiling ratio is represented over the AOI with color coded daily average soiling ratio values. Five exemplary fits for different average soiling ratio bins are shown. As it is the case for the PSA, we neglected AOIs greater 70°, excluding 5 % of the total energy yield.

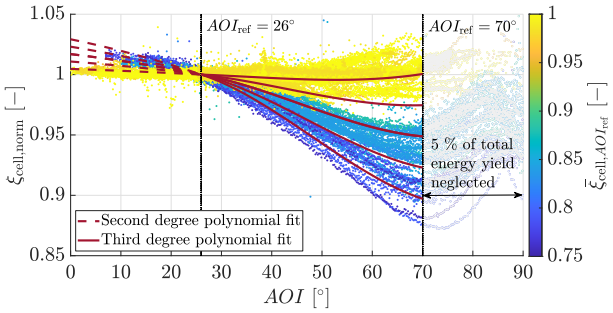

FIG. 11. Normalized T_L-cloudfiltered soiling ratio vs. AOI with color coded $\bar{\xi}_{\text{cell},AOI\text{ref}}$ of fixed PV modlues . Reference AOI bin: 24° - 28°. Also 5 exemplary polynomial fits $f(AOI, \xi_{\text{cell}})$ per fit range through selected bins using the linear regression results are shown.

In figure 12 the coefficients of the second-order polynomials are plotted against the daily average soiling ratio bins. A linear regression was performed, to determine a functional relationship between every single fitting coefficient and the daily average soiling ratio bins. In this manner, regression coefficients for arbitrary bin limits or higher soiling ratio values can be extrapolated that have not occurred.

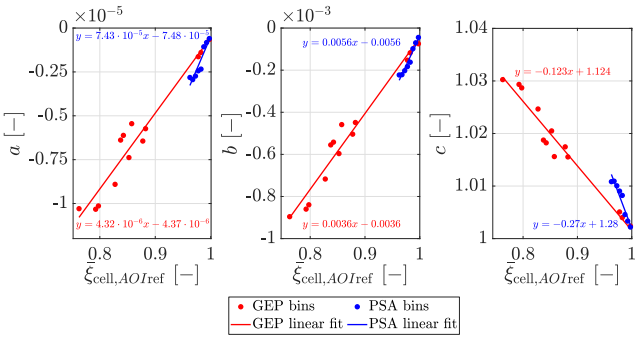

FIG. 12. Fit coefficients of polynomial of order 2 over daily average soiling ratio bins for the PSA (blue) and the GEP (red). Linear fits were generated to find a functional relationship between each fit coefficient and $\bar{\xi}_{\text{cell},AOI\text{ref}}$

An exemplary linear regression for the fitting parameter a of the polynomial of order 3 is shown in figure 13. We compare the linear regression results for the GEP and the PSA and find that there is a discrepancy in the slope of both linear fits. This is due to the different tilt angles used in both setups and the thus resulting AOI occurrence. Changes in the surface-azimuth angle would also lead to other AOI distributions. Also, the tilt and orientation of an inclined surface have proven to have a major impact on dust accumulation[28,29].

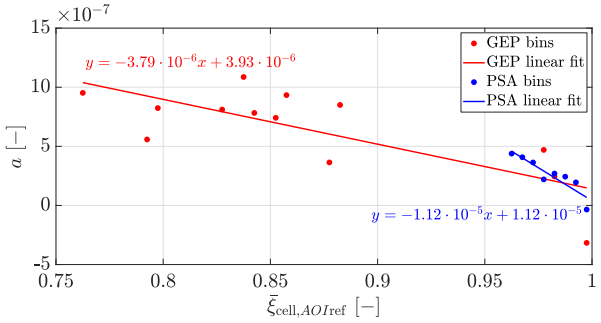

FIG. 13. Fit coefficient a of polynomial of order 3 over daily average soiling ratio bins for the PSA (blue) and the GEP (red). Linear fits were generated to find a functional relationship between each fit coefficient and $\bar{\xi}_{\text{cell},AOI\text{ref}}$

E. Dependency on the diffuse fraction of incident light

Up to this point we analyzed only data-points taken at sunny conditions. In this section we want to characterize the AOI-influence on soiling rate measurements taken at hazy to shady irradiance conditions. The soiling ratio is shown against the AOI for $T_L > 10$ in figure 14. The characteristic of the plots for sunny data points is completely lost. Nearly no AOI dependency can be identified. As this plot only shows very high T_L levels, a transition from sunny to shady has to be found. Based on the observed data at the PSA, we assume a lower boundary $T_{L,\text{ref1}}$ of 4. Values measured at lower AOI correspond to sunny conditions. We assume an upper boundary $T_{L,\text{ref2}}$ of 7 corresponding to a completely overcast sky. All values in between these boundaries correspond to a transition from sunny to shady conditions, where the cloud/dust transmission decreases with increasing T_L. These boundaries can vary according to the geographic location, the altitude and the climate.

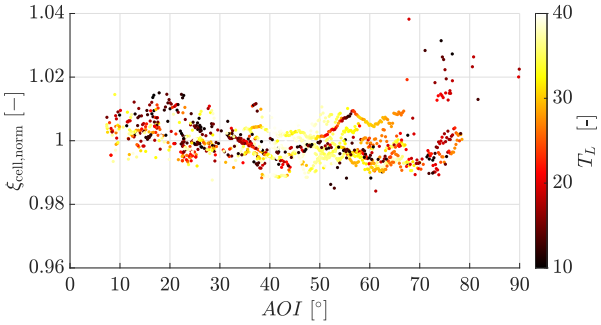

FIG. 14. Scatter plot of normalized soiling ratio vs. AOI for cloudy conditions with color coded T_L and $0.96 < \bar{\xi}_{\text{cell},AOI\text{ref}} < 0.97$ for the fixed cells with textured glass at the PSA

F. Adaptation function for automatic sensors

In this section the AOI- and diffuse radiation adaptation method for the DustIQ and potentially other automatic soiling sensors with proprietary light sources is presented. The proposed adaptation equation can be written as follows:

$$\xi_{\mathrm{DIQ,calib,corr}} = \xi_{\mathrm{DIQ,uncorr}} \cdot c_{\mathrm{DIQ}} \cdot f(\theta, \xi_{\mathrm{cell}})^{\frac{1}{T_L - T_{L,\mathrm{ref}} + 1}} \quad (11)$$

The adaptation takes account of c_{DIQ} that is the ratio of the measured factory calibrated soiling ratio to the soiling ratio measured during the DustIQ's local dust slope calibration at AOI_{ref}. The sunny adaptation function $f(\theta, \xi_{\mathrm{cell}})$ is derived through polynomial fitting as described above. The exponent describes the transition from sunny and hazy to totally covered skies. For sunny cases the exponent is 1, and decreases with growing T_L as long as the calculated T_L is inside the sunny to shady transition boundaries. For large T_L, the adaptation function approaches 1 ($T_L >\sim 10$). This behavior can be observed in figure 15 that shows 4 correction functions for different T_L levels and a reference soiling ratio between 0.96 and 0.97. It can be seen that the correction is dampened with increasing T_L.

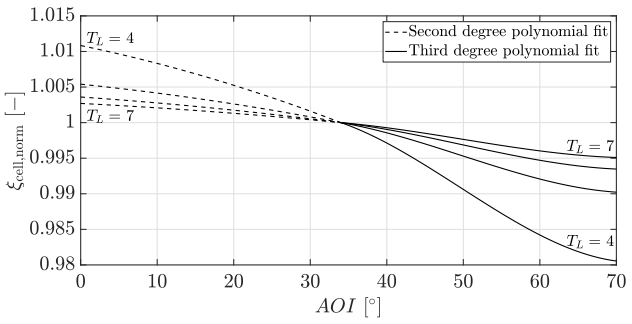

FIG. 15. Correction function for different T_L levels and $0.96 < \xi_{\mathrm{cell},AOI\mathrm{ref}} < 0.97$ as determined for data measured at CIEMAT's PSA. AOI-dependence on low T_L and increased soiling levels is more expressed and approximates unity for large T_L.

IV. RESULTS AND DISCUSSION

Figure 16 shows a two day episode of DustIQ data as corrected with the proposed method in comparison to the reference soiling ratio from the reference cell setup at CIEMAT's PSA. It can be seen that for sunny days, the adaptation method works well and reproduces the angular soiling ratio dependency for the DustIQ. An episode with strongly fluctuating and partially jumping T_L can be seen in the inset in the upper right corner of Figure 16. $\xi_{DIQ,corr}$ follows the reference soiling ratio for low $T_L < T_{L,ref}$ ranges and jumps towards the uncorrected DustIQ signal for $T_L > T_{L,ref}$. The reference PVRC soiling ratio is also strongly influenced by the increase in T_L, in that they also fluctuate and assume higher values as the DustIQ's raw signal. Therefore a bias remains between the two measurements under turbid conditions. The correction works in attenuating the AOI effect for increasing T_L values, but does not perfectly reproduce the PVRC soiling ratio. In figure 17 the corrected DustIQ soiling ratio is plotted

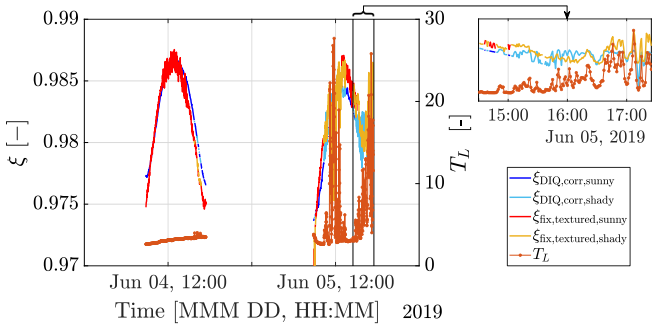

FIG. 16. AOI and diffuse radiation adapted DustIQ (blue - sunny, light blue - shady) and fixed textured PVRC (red - sunny, yelow – shady) soiling ratios over time at the PSA. The Linke turbidity coefficient is plotted on the right y-axis. Only soiling ratios at AOI < 70° are considered.

over time together with the Linke turbidity. It can be seen that the adaptation works well for episodes with sunny conditions. Once irradiance conditions start to fluctuate, the adaptation cannot be perfect any more due to the high noise in the reference soiling ratio. Suppressing the AOI-correction at these intermittent episodes brings $\xi_{\mathrm{DIQ,corr}}$ closer to the reference. T_L is a good indicator for episodes where the adaptation should be omitted.

The city of Ben Guerir is subject to a mediterranean climate influenced by the near desert. Dust particles mainly originate from surrounding semi-arid grounds and the Saharan desert as well as open-pit phosphore-mines located only 10 km away that produce large amounts of calcitic dusts. Also, the occurrence of dust storms and of red rain contributes to the higher soiling levels observed at GEP. An important difference of the GEP measurement setup is the different reference soiling ratio measurement that is performed with modules at GEP as opposed to the reference cells used at CIEMAT's PSA. Modules react more sensitively to inhomogeneous distributions of soiling over its surface due to mismatching effects caused by partial shading. In these conditions, the soiling found on the small DustIQ measurement surface can be considered a random sample of a broad soiling ratio distribution and might differ strongly in periods from the modules' soiling ratio.

The fact that no local dust slope calibration has been performed for the DustIQ in GEP additionally increases the offset between the DustIQ and reference soiling ratio seen in Figures 17 and 18. Although the general trends of the measured soiling ratios should be similar, their absolute values differ more as those at CIEMAT's PSA. During episodes where irradiance conditions fluctuate between cloudy and sunny, the module's soiling ratio shows increased noise in comparison to the reference cells employed at CIEMAT's PSA.

Due to the atmospheric conditions at GEP, the determination of f by fitting has been performed for higher average T_L levels. Therefore, $T_{L,\mathrm{ref}}$ has been set to 6 for GEP in order to

avoid under-correction of the DustIQ signal for low T_L at GEP.

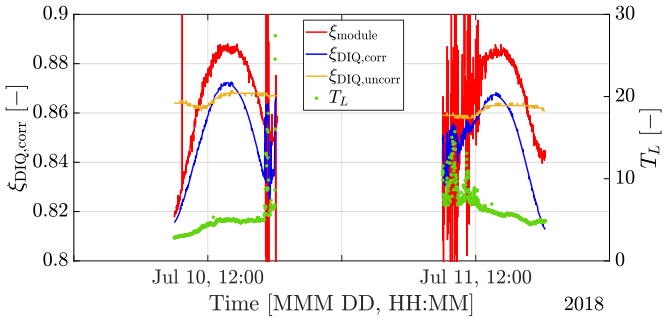

FIG. 17. DustIQ (blue - AOI and diffuse radiation adapted, yellow - uncorrected) and module (red) soiling ratio over time at GEP. The Linke turbidity coefficient is shown in green on the right y-axis. Only soiling ratios for AOI < 70° are considered.

Figure 18 shows a scatter diagram comparing the DustIQ soiling rate data before (left) and after (right) the application of the AOI-adaptation method to the PVRC reference soiling ratio for a one week measurement interval. The RMSD has decreased from 0.0065 to 0.0024 by the adaptation method for this data interval. The AOI during measurement is shown in the color of the datapoints. It can be seen that the data-points with higher AOI better agree with the PVRC reference thanks to the adaptation. Power plants with high DC/AC ratios, i.e. where the solar array nominal DC output power is higher compared to the nominal AC output of the inverters, tend to clip power on the DC side during high irradiance conditions that more likely appear at low AOI ranges. During clipping, the soiling ratio does not play a role any more for the electrical power output of the plant, as enough production is available anyways[30]. In this application case, the accuracy increase at higher AOI becomes more important. using uncorrected DustIQ soiling ratio data could lead to an overestimation of the power output.

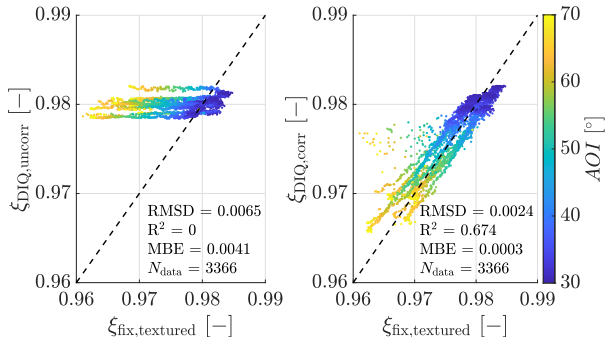

FIG. 18. Scatter plot for uncorrected (l.)/corrected (r.) DustIQ and fix textured PVRC soiling ratios measured between 06.06.2019 and 12.06.2019 at CIEMAT's PSA. *AOI* is shown in color.

Figure 19 shows a scatter density-plot with the same x- and y-axis as above, now for a larger time interval of 3 months. The data density is shown in color. A similar behaviour as in Figure 18 can be observed: the lower PVRC soiling ratios that are not reproduced by the DustIQ's raw signal are populated well after the application of the adaptation method. the RMSD in this measurement time frame can be reduced from 0.0051 to 0.0028 by the presented method. The bias is reduced to a third when compared to the uncorrected DustIQ soiling ratio.

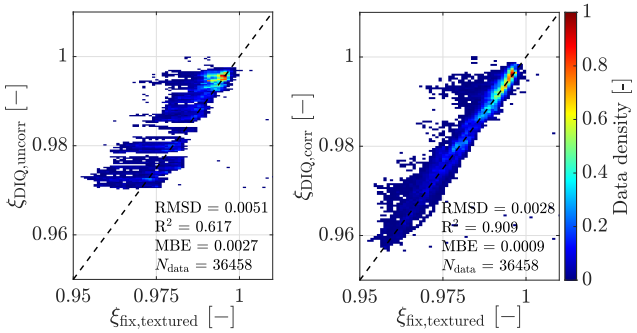

FIG. 19. Density plot comparing uncorrected (l.)/corrected (r.) DustIQ and fix textured PVRC soiling ratios measured from 12.03.2019 until 12.06.2019 at CIEMAT's PSA. Color shows the data density

Figure 20 shows a scatter plot with the *AOI* shown in color for a measurement period at GEP analogous to figure 18. Due to the higher measurement uncertainty in the reference soiling ratio with PV-modules and the significantly lower soiling ratio range found at GEP, the data show a generally broader distribution and noise. Nevertheless, a similar behavior as at PSA can be found: uncorrected DustIQs tend to overestimate the soiling ratio for high *AOI* levels. The adaptation method makes the DustIQ data fit the reference data better. The RMSD can be reduced from 0.52 to 0.49 due to the adaptation. Two qualitatively distinct measurement episodes can be identified with different bias. One of which in the upper right corner of the graph, the other more centrally located. There seems to be a offset that can originate from a change in the soiling distribution on the reference module at a certain point in time causing the soiling ratios to compare differently for the two situations. This offset dominates the bias error after adaptation. The *AOI* behaviour is represented better after the adaptation than before for both measurement sites.

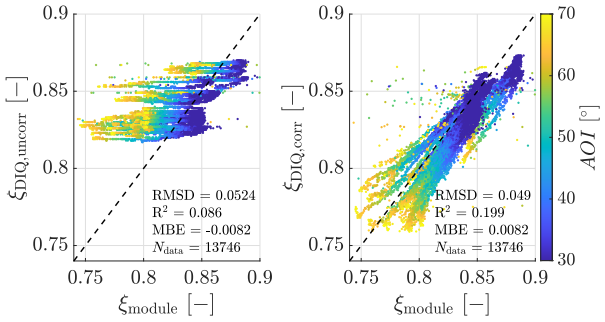

FIG. 20. Scatter plot between uncorrected (l.)/corrected (r.) DustIQ and module soiling ratio (08.07.18'-21.08.18' at IRESEN's GEP) with color coded *AOI*

V. CONCLUSION

An analysis of the AOI-behaviour of a soiling-measurement setup consisting of PV reference cells (PVRC) and a DustIQ soiling sensor is presented. The PVRC soiling ratio output is used as a reference as it best reproduces the production of PV for same orientations. For sunny measurement days, the AOI-behavior of the PVRC soiling ratio is characterized by fitting the normalized soiling ratio as a function of the AOI. The soiling ratio is normalized against the soiling ratio measured at a reference AOI of same measurement days. Different fitting functions are found for different reference soiling ratio bins. The fitting parameters are parameterized in order to find fit functions for all reference soiling ratios. When irradiance conditions transition from clear to hazy and clouded, the AOI-dependency becomes less pronounced. The fit functions are therefore damped for diffuse conditions as a function of the Linke Turbidity. The latter can be derived from parallel GHI or plane of array irradiance measurements.

Based on this analysis, an adaptation method applicable for active soiling sensors, that do not include the AOI effect on the soiling ratio in their output signal is presented. The method is widely applicable as the correction depends only on the AOI and the Linke Turbidity. The thus corrected DustIQ signal reproduces the daily course of the soiling ratio as measured with the PVRC. The correction significantly increases the agreement between both parameters and reduces the RMSD between both signals from 0.0051 to 0.0028.

The method can improve the accuracy of yield analysis calculations and performance analysis based on automatic dust sensors. Especially if plants with high DC/AC ratios resulting in increased clipping at high irradiance conditions are considered. As high irradiance is more likely to appear at low AOI, soiling ratio at low AOI become less important. Improving the accuracy of soiling ratio measurements for high AOI facilitates a better separation of parameters for more irradiance conditions and AOI and improve performance analysis studies.

ACKNOWLEDGMENTS

This research is part of SOLWARIS project that has received funding from the European Union's Horizon 2020 research and innovation programme under the Gran Agreement No. 792103

REFERENCES

[1] K. Ilse, L. Micheli, B. W. Figgis, K. Lange, D. Daßler, H. Hanifi, F. Wolfertstetter, V. Naumann, C. Hagendorf, R. Gottschalg, *et al.*, "Techno-economic assessment of soiling losses and mitigation strategies for solar power generation," Joule **3**, pp. 2303–2321 (2019).

[2] N. Martín and J. M. Ruiz, "A new model for PV modules angular losses under field conditions," International Journal of Solar Energy **22**, pp. 19–31 (2002).

[3] D. L. King, W. E. Boyson, and J. A. Kratochvill, "Photovoltaic array performance model," Tech. Rep. (Sandia National Laboratories, 2004).

[4] J. Zorrilla-Casanova, M. Piliougine, J. Carretero, P. Bernaola, P. Carpena, L. Mora-Lopez, and M. Sidrach-de Cardona, "Analysis of dust losses in photovoltaic modules," (2011) pp. 2985–2992.

[5] J. John, V. Rajasekar, S. Boppana, S. Tatapudi, and G. Tamizhmani, "Angle of incidence effects on soiled PV modules," (San Diego, California, United States, 2014) p. 91790D.

[6] B. Figgis, A. Ennaoui, S. Ahzi, and Y. Rémond, "Review of pv soiling measurement methods," in *2016 International Renewable and Sustainable Energy Conference (IRSEC)* (2016) pp. 176–180.

[7] R. Sharma, "Effect of obliquity of incident light on the performance of silicon solar cells," Elsevier Ltd. (2019).

[8] N. Martín, F. Chenlo, E. Mejuto, F. Soriano, S. Temprano, and M. C. Alonso-García, "Validating an angular of incidence losses model with different PV technologies and soiling conditions," (2012).

[9] P. Nepal, M. Korevaar, H. Ziar, O. Isabella, and M. Zeman, "Accurate soiling ratio determination with incident angle modifier for PV modules," IEEE Journal of Photovoltaics **9**, 295–301 (2019).

[10] L. Dunn, M. Gostein, and K. Emery, "Comparison of pyranometers vs. PV reference cells for evaluation of PV array performance," in *2012 38th IEEE Photovoltaic Specialists Conference* (IEEE, Austin, TX, USA, 2012) pp. 002899–002904.

[11] L. Dunn, B. Littmann, J. R. Caron, and M. Gostein, "PV module soiling measurement uncertainty analysis," in *2013 IEEE 39th Photovoltaic Specialists Conference (PVSC)* (IEEE, Tampa, FL, USA, 2013) pp. 0658–0663.

[12] M. Korevaar, J. Mes, T. Bergmans, D. van Velsen, K. Dalu, and X. van Mechelen, "DustIQ soiling monitoring field data," , 40 (2018).

[13] "Photovoltaic System Performance - Part 1: Monitoring," Standard IEC 61724-1:2017 (IEC International Standards, 2017).

[14] L. Viel, "Solar-Einstrahlungssensor SOZ-03 Datenblatt," Tech. Rep. (NES Mess- und Meldesysteme, 2017).

[15] L. Viel, "Solar-Einstrahlungssensor SOZ-03 Kalibrierungszertifikat," Tech. Rep. (NES Mess- und Meldesysteme, 2017).

[16] Kipp und Zonen, "DustIQ Soiling Measurement Instruction Manuel," `https://www.kippzonen.com/Download/996/Declaration-of-Conformity-DustIQ-0386910-and-0386915-models` (2019), accessed: 16 November 2020.

[17] "Local dust calibration for the DustIQ soiling measurement system," `https://www.pv-magazine.com/2018/11/20/local-dust-calibration-for-the-dustiq-soiling-measurement-system/` (November 20, 2018), accessed: 16 November 2020.

[18] Kipp und Zonen, "DustIQ Calibration Procedure," `https://www.kippzonen.com/Download/999/DustIQ-Calibration-Procedure-0386910-and-0386915-models`, accessed: 16 November 2020.

[19] C. Demain, M. Journée, and C. Bertrand, "Evaluation of different models to estimate the global solar radiation on inclined surfaces," Renewable Energy **50**, pp. 710–721 (2012).

[20] C. C. Y. Ma and M. Iqbal, "Statistical comparison of models for estimating solar radiation on inclined surfaces," Solar Energy **31**, pp. 313–317 (1983).

[21] "Albedo measurements," `http://www.climatedata.info/forcing/albedo/]`, accessed: 16 November 2020.

[22] P. Ineichen and R. Perez, "A new airmass independent formulation for the Linke turbidity coefficient," Solar Energy **73**, pp. 151–157 (2002).

[23] M. Lefèvre, A. Oumbe, P. Blanc, B. Espinar, B. Gschwind, Z. Qu, L. Wald, M. Schroedter-Homscheidt, C. Hoyer-Klick, A. Arola, A. Benedetti, J. Kaiser, and J.-J. Morcrette, "Mcclear: A new model estimating downwelling solar radiation at ground level in clear-sky conditions," Atmospheric Measurement Techniques **6**, 2403–2418 (2013).

[24] C. N. Long and T. P. Ackerman, "Identification of clear skies from broadband pyranometer measurements and calculation of downwelling shortwave cloud effects," Journal of Geophysical Research (2000).

[25] F. Kasten and A. T. Young, "Revised optical air mass tables and approximation formula," Appl. Opt. **28**, pp. 4735–4738 (1989).

[26] S. Wilbert, S. Kleindiek, F. Vignola, A. Habte, B. Nouri, Geuder, and M. N., Schwandt, "Uncertainty of rotating shadowband irradiometers and Si-Pyranometers including the spectral irradiance error," SolarPACES. Cape Town, South Africa (2015).

[27] N. Hanrieder, M. Sengupta, Y. Xie, S. Wilbert, and R. Pitz-Paal, "Modeling beam attenuation in solar tower plants using common dni measurements," Solar Energy vol. 129 , pp. 244–255 (2016).

[28] B. Figgis, A. Ennaoui, S. Ahzi, and Y. Rémond, "Review of PV soiling

particle mechanics in desert environments," Renewable and Sustainable Energy Reviews **76**, 872–881 (2017).

[29] A. Sayyah, M. N. Horenstein, and M. K. Mazumder, "Energy yield loss caused by dust deposition on photovoltaic panels," Solar Energy **107**, 576–604 (2014).

[30] J. Dolan, D. S. L. Dolan, V. Prodanov, and J. Puckett, "Power loss due to photovoltaic module soiling in a california utility scale system," in *2019 9th International Conference on Power and Energy Systems (ICPES)* (2019) pp. 1–5.